PAPER • OPEN ACCESS

Enhanced understanding of non-axisymmetric intrinsic and controlled field impacts in tokamaks

To cite this article: Y. In *et al* 2017 *Nucl. Fusion* **57** 116054

View the article online for updates and enhancements.

Enhanced understanding of non-axisymmetric intrinsic and controlled field impacts in tokamaks

Y. In[1], J.-K. Park[2], Y.M. Jeon[1], J. Kim[1], G.Y. Park[1], J.-W. Ahn[3], A. Loarte[4], W.H. Ko[1], H.H. Lee[1], J.W. Yoo[1], J.W. Juhn[1], S.W. Yoon[1], H. Park[1,5] and 3D Physics Task Force in KSTAR

[1] National Fusion Research Institute, Daejeon, Republic of Korea
[2] Princeton Plasma Physics Laboratory, Princeton, New Jersey, United States of America
[3] Oak Ridge National Laboratory, Oak Ridge, Tennessee, United States of America
[4] ITER organization, St. Paul Lez Durance, France
[5] Ulsan National Institute of Science and Technology, Ulsan, Republic of Korea

E-mail: yongkyoon@nfri.re.kr

Abstract

An extensive study of intrinsic and controlled non-axisymmetric field (δB) impacts in KSTAR has enhanced the understanding about non-axisymmetric field physics and its implications, in particular, on resonant magnetic perturbation (RMP) physics and power threshold (P_{th}) for L–H transition. The $n = 1$ intrinsic non-axisymmetric field in KSTAR was measured to remain as low as $\delta B/B_0 \sim 4 \times 10^{-5}$ even at high-beta plasmas ($\beta_N \sim 2$), which corresponds to approximately 20% below the targeted ITER tolerance level. As for the RMP edge-localized-modes (ELM) control, robust $n = 1$ RMP ELM-crash-suppression has been not only sustained for more than ~90 τ_E, but also confirmed to be compatible with rotating RMP. An optimal window of radial position of lower X-point (i.e. $R_x = 1.44 \pm 0.02$ m) proved to be quite critical to reach full $n = 1$ RMP-driven ELM-crash-suppression, while a constraint of the safety factor could be relaxed ($q_{95} = 5 \pm 0.25$). A more encouraging finding was that even when R_x cannot be positioned in the optimal window, another systematic scan in the vicinity of the previously optimal R_x allows for a new optimal window with relatively small variations of plasma parameters. Also, we have addressed the importance of optimal phasing (i.e. toroidal phase difference between adjacent rows) for $n = 1$ RMP-driven ELM control, consistent with an ideal plasma response modeling which could predict phasing-dependent ELM suppression windows. In support of ITER RMP study, intentionally misaligned RMPs have been found to be quite effective during ELM-mitigation stage in lowering the peaks of divertor heat flux, as well as in broadening the 'wet' areas. Besides, a systematic survey of P_{th} dependence on non-axisymmetric field has revealed the potential limit of the merit of low intrinsic non-axisymmetry. Considering that the ITER RMP coils are composed of 3-rows, just like in KSTAR, further 3D physics study in KSTAR is expected to help us minimize the uncertainties of the ITER RMP coils, as well as establish an optimal 3D configuration for ITER and future reactors.

1. Introduction

A seemingly negligible level ($\delta B/B_0 \sim 10^{-4}$) of intrinsic non-axisymmetric field (δB) has been proven to be quite a significant challenge for high-β plasmas [1, 2], while an introduction of significant level ($\delta B/B_0 \sim$ up to 10^{-3}) of controlled δB has been confirmed to be effective in controlling edge-localized-mode (ELMs) [3]. (Here, B_0 is the magnetic field strength at geometric center of tokamak, while β refers to a ratio of plasma kinetic pressure to applied magnetic field pressure.) Despite substantial progress that have been made for the last couple of decades, the understanding of such a 'double-sided' impact of non-axisymmetric field on stability and transport needs to be enhanced for ITER and future reactors [4–6]. In general, intrinsic non-axisymmetric field (often called 'error field (EF)') is unintentionally introduced during plasma operation, and should be corrected for high-performance plasmas [7]. In contrast, we purposely apply controlled non-axisymmetric fields to maximize the benefits of stochastic fields (e.g. resonant magnetic perturbation (RMP) to control ELMs) [8]. In that regard, when an intrinsic non-axisymmetric field can be reduced to an order of magnitude lower level than a typical level (i.e. $\delta B/B_0 \sim 10^{-5}$, rather than 10^{-4} [9, 10]), we would be in a better position to resolve various non-axisymmetric field physics issues on stability and transport in tokamaks unambiguously.

Recently, the KSTAR has been diagnosed with such an extremely low intrinsic EF ($\delta B/B_0 \sim 10^{-5}$) [10], as well as with unprecedentedly low level of toroidal field ripple ($\delta_{TF} = 0.05\%$) [11]. As a result, the KSTAR is keen to take advantage of this opportunity, clarifying various plasma responses against externally controlled non-axisymmetric fields without being influenced by any residual non-axisymmetry.

So far, in KSTAR, no need of dedicated EF correction has been identified in its routine operation, even at relatively high-β plasmas (e.g. $\beta_N \sim 2$, where β_N (% mT/MA) is defined as $\beta/(I_p/aB_T)$ with plasma current I_p (MA), minor radius a (m), and toroidal magnetic field B_T (T)) [12]. The merit of low intrinsic EF is potentially identified by its accessibility to low q_{95} (~2) plasmas, which is known to be notoriously difficult without high quality EF correction and/or feedback control in conventional devices [13, 14]. Since a low level of intrinsic non-axisymmetry leads to a weak influence of neoclassical toroidal viscosity (NTV), faster plasma rotation (up to Mach number ~0.8 (deuterium)) in KSTAR [15], in comparison with other devices of similar size at nearly the same level of heating input power, may be easily understood. According to a newly recognized NTV study [16], routinely observed edge rotation pedestal, and strong edge rotation shear in KSTAR would be also attributable to such a low level of intrinsic non-axisymmetry, allowing for a formation of momentum transport barrier at edge. Furthermore, with the help of the

state-of-the-art imaging diagnostic [17], we have diagnosed the nonlinear interaction of ELM and turbulent eddies driven by $n = 1$ RMP for the first time, which might explain how RMP-driven stochastic field would alter the dynamics of ELMs [18].

Now, combining an improved axisymmetric control capability, the KSTAR has significantly enhanced the understandings of controlled non-axisymmetric field study, in particular, on RMP physics and power threshold (P_{th}) for L–H transition. For example, as will be discussed later, the $n = 1$ RMP-driven ELM-crash-suppression has been not only sustained for more than ~90 τ_E, but also confirmed to be compatible with rotating RMP [19]. Also, a systematic scan of power threshold for L–H transition shows that KSTAR indeed appears lower than the projected level by a multi-device empirical scaling, as potentially another evidence of the merit of low intrinsic non-axisymmetry [20].

In section 2, a brief summary of the intrinsic $n = 1$ non-axisymmetric field measurements in KSTAR will be given, showing its β dependence in the order of $\delta B/B_0 \sim 10^{-5}$. In section 3, the controlled non-axisymmetric field study results will be presented and discussed with an emphasis on RMP-driven ELM control, and L–H power threshold study. In section 4, the impact of intentionally misaligned ITER-like RMP configurations on divertor heat flux footprints is assessed and discussed. In section 5, the relevant topical issues and prospects will be discussed. In section 6, a brief summary is given.

2. Intrinsic non-axisymmetric fields

The full 3D structure of the $n = 1$ intrinsic EF in KSTAR has been investigated using in-vessel control coils (IVCC) in various plasma conditions, according to a multi-year plan. For now, based on the middle row scan, a complete set has been made in low, intermediate, and relatively high β plasmas respectively.

2.1. Resources for non-axisymmetric field study in KSTAR

The KSTAR has three rows (Top/Middle/Bottom) of versatile IVCC (capable of up to $n = 2$) with 2 turns in low field side [21], whose configuration is similar to that of the planned ITER RMP coils (capable of up to $n = 4$). Unlike other tokamaks equipped with two (Top/Bottom) rows of RMP coils, the KSTAR is the only major tokamak that has in-vessel mid-plane RMP coils. Hence, any uncertainties involved in ITER in-vessel mid-RMP coils can be directly addressed in KSTAR. Incorporating broadband switching power amplifiers (SPA) capable of up to 5 kA/turn in DC to 1 kHz, various 3D configurations with $n = 1$ and/or $n = 2$ fields can be applied in conjunction with three dozens of assorted patch panels in KSTAR [22]. Besides, along with an upgraded magnetic
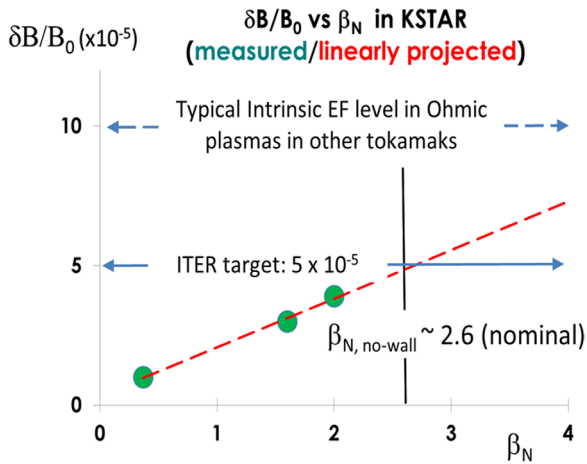
Figure 1. $n = 1$ intrinsic error field measurements and linear projection [12]. According to mid-IVCC compass scans on low-β ohmic, intermediate-β H-mode, and relatively high-β H-mode discharges (in green) respectively, a linear dependence of error field on β_N is extrapolated up to higher β_N (in red). Reproduced courtesy of IAEA. Figure from [12]. Copyright 2017 IAEA.

diagnostic (i.e. magnetic probes installed on passive plates), various plasma responses for 3D field physics study can be directly diagnosed by the state-of-the-art diagnostics, such as electron cyclotron emission imaging (ECEI) [17] and microwave interferometry (MIR) [23].

2.2. Measurement of $n = 1$ intrinsic non-axisymmetric field

Figure 1 shows a summary of the $n = 1$ intrinsic EF in low/intermediate/high-β plasmas in KSTAR. In particular, it is to be noted that the $n = 1$ intrinsic EF in high-β plasmas ($\beta_N \sim 2$) was measured to be as low as $\sim 4 \times 10^{-5}$ B_0, consistent with a linear extrapolation of the EF measurements on low-β [10], and intermediate-β plasmas. This corresponds to approximately 20% below the targeted ITER tolerance level (5×10^{-5} B_0) [4]. Unlike a typical 'compass scan' that uses either mode-locking or angular momentum variations [24], the $n = 1$ intrinsic EF at high-β plasmas was determined based on rotation collapse due to $n = 1$ field penetration [12]. Hence, a linear projection suggests that the $n = 1$ intrinsic EF would remain low enough for KSTAR to easily reach the no-wall stability limit (nominally $\beta_N \sim 2.6$), and possibly up to $\beta_N \sim 3$ (due to kinetic effects (e.g [25])) without dedicated EF correction. While the identification of $n > 1$ intrinsic EF based on non-axisymmetric plasma response is limited in KSTAR due to the insufficient number of the toroidal coil sectors, no evidence of $n > 1$ EF has been found yet.

3. Controlled non-axisymmetric field impacts on stability and transport

In ITER and future reactors, the presence of ELMs poses substantial risks, in that the out-bursting particle and heat fluxes could damage the divertor and plasma facing components in an uncontrolled manner [8]. Among several schemes to control such ELMs, the application of RMP, which creates

stochastic magnetic field to divert the ELM onset condition, has been proven to be quite effective to either suppress or mitigate ELMs. Although it is ideal to achieve RMP-driven ELM-crash-suppression, rather than ELM-crash-mitigation, only a handful of devices, including KSTAR, have reported full ELM-suppression at most up to several seconds so far [27]. Thus, it is imperative to not only establish a robust path to RMP-driven ELM control capability, but also clarify the relevant physics mechanism, in particular, about full ELM suppression. In that regard, the KSTAR has now secured a path to access robust $n = 1$ RMP ELM control, while demonstrating the prediction capability of optimal 3D configuration necessary for $n = 1$ RMP-driven ELM suppression. Also, in 3D transport study, a merit of low intrinsic non-axisymmetry has been systematically quantified in terms of power threshold of L–H transition.

3.1. Stationary ELM crash suppression using low-n RMPs

As one of the important milestones, KSTAR has demonstrated a record-long (>10 s, more than 90 τ_E) sustainment of RMP-driven ELM-crash-suppressed H-modes, as shown in figure 2. In addition to a typical ELM-suppressed discharge in the past in KSTAR (near $q_{95} \sim 6$), a very wide ELM suppression window of the safety factor (q_{95}) has been identified near 5.0 ± 0.25 with a level of RMP field $\delta B_{RMP}/B_T \sim (5–7) \times 10^{-4}$ at pedestal top (with magnetic field $B_T = 1.8$ T, plasma current $I_P = 0.5$ MA, and external NBI heating power $P_{NBI} \sim 2.8$ MW) with collisionality $\nu^* \sim 0.2–0.25$ (assuming $Z_{eff} = 1$) [19]. Such superb performance of RMP-driven ELM-crash-suppression has been ascertained to be very reproducible (with more than 100 discharges). More importantly, the methodology we have developed now guides us to a new frontier of RMP physics in terms of both accessibility and robustness. Specifically, we have found a distinctive shape dependence of radial position of lower X-point ($R_x = 1.44$ m) within ± 0.02 m, which corresponds to the lower triangularity of $\delta_l = 0.74 \pm 0.04$ [19].

However, as shown in figure 3, such 'performance-oriented' configuration (in black) cannot be easily diagnosed by a divertor camera overlooking downward from the top [28], in that the outer striking point would reside on the vertical leg of the divertor. Hence, taking into account the spatially limited view of infra-red camera for divertor heat flux measurements, another set of systematic parameter scans was conducted with $R_x = 1.39$ m nearly fixed (in red in figure 3), in which the outer strike point would be located at the center of the divertor. Fortunately, another optimal window of R_x was found in the vicinity of the original R_x (at 1.44 m in black) with relatively minor changes of other plasma parameters at the expense of much more challenging operational sensitivities. As a result, the 2nd optimal group with more strict constraints have been found at $q_{95} = 4.95 \pm 0.05$, and $R_x = 1.39 \pm 0.01$ m, (i.e. $\delta_l = 0.85 \pm 0.02$) respectively. In fact, figure 4 shows such a newly established ELM-crash-suppression discharge, whose optimal lower R_x is positioned at 1.39 m. Although the duration ($\sim 50 \tau_E$) of ELM-suppressed stage is shorter than that of the performance-oriented configuration (as shown in figure 2), the
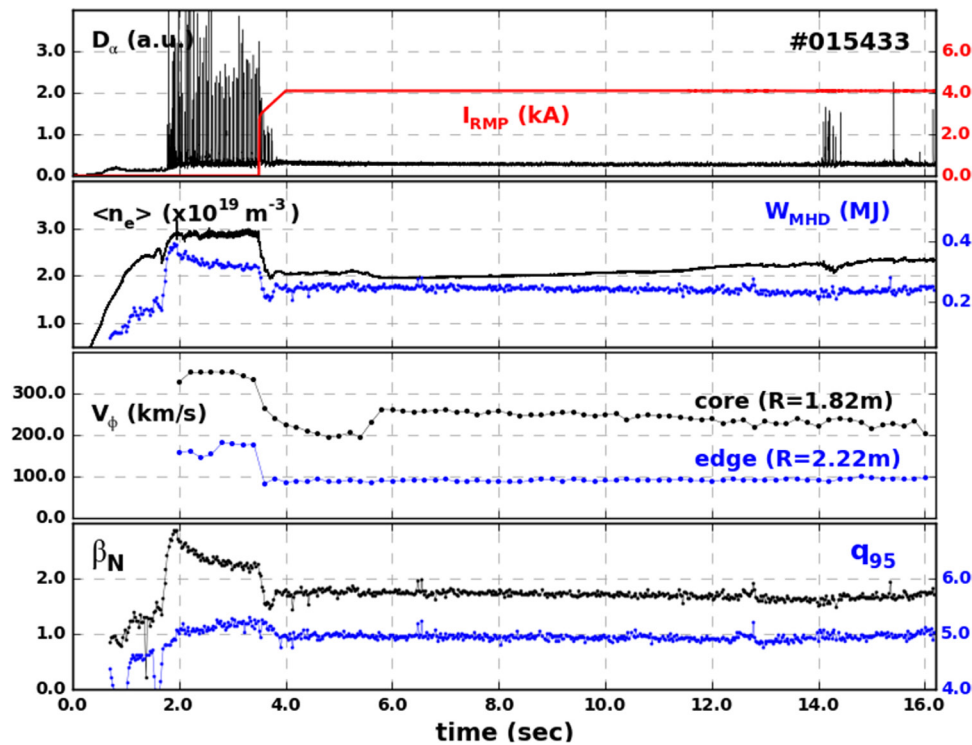
Figure 2. Demonstration of quasi-stationary (>90 τ_E) ELM suppression with $n = 1$ RMP (whose 3-row configuration is similar to what is planned for ITER). Shown from top to bottom in order are the time traces of (i) D_α (lowest-energy spectral line of deuterium Balmer series) signal at divertor, and RMP coil current (red), (ii) density and stored energy (blue), (iii) plasma rotation at core and edge (blue), and (iv) normalized β, and safety factor, q_{95} (blue) respectively.

availability of divertor heat flux measurement during ELM-controlled periods enabled us to directly diagnose the 3D configuration impact on the divertor. Figure 5 shows the divertor heat flux footprints measured using an infra-red camera during $n = 1$ RMP-driven ELM-crash-suppression from 3.2 s to 8.7 s on 16661 shown in figure 4. The striation patterns consist of the axisymmetric peak ($R \sim 1.45$ m), and $n = 1$ non-axisymmetric peak ($R \sim 1.47$ m), while each peak is below ~1.2 MW m^{-2} at $P_{NBI} = 3.4$ MW with $\nu^* \sim 0.3$–0.4 (assuming $Z_{eff} = 1$), as summarized in the right figure of figure 5. Throughout this discharge, a peak of the axisymmetric lobe remains higher than that of non-axisymmetric lobe. Interestingly, even during ELM-suppressed stage, there is a noticeable evolution of the non-axisymmetric peak, which appears to have taken a few seconds to be built up from the early stage (at 3.5 s marked at 'A'), prior to the fully grown stage (at 5.0 s, up to a similar level marked at 'B'). This suggests there is another transport process to establish a heat flux channel from edge plasma to divertor, which could be virtually independent of any onset criteria of ELM suppression.

Similarly, we have confirmed the validity of the operational approach even on the $n = 2$ (near $q_{95} \sim 4$) RMP ELM control, but so far observed the marginal suppression or strong mitigation frequently, rather than full suppression. While a further study needs to be done, we are speculating the limited capability of $n = 2$ phasing adjustment in KSTAR could be partially responsible for non-optimal $n = 2$ RMP coupling to edge plasmas. Here, the phasing refers to the toroidal phase difference between adjacent rows. Since the existing IVCCs are composed of 4 coils in a row, an arbitrary $n = 2$ toroidal
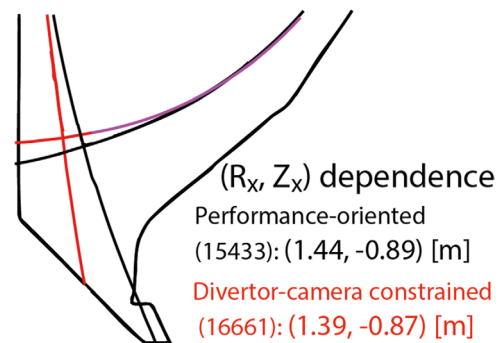

Figure 3. Two groups of optimal *X*-points for $n = 1$ RMP ELM control. Although performance-oriented configuration (in black) cannot be easily diagnosed due to the unfavourable outer striking point landing on the vertical divertor leg, another group of configuration (in red) has been found to be optimal for both RMP control and heat flux measurement.

phase cannot be easily accommodated. As a result, the $n = 2$ phasing adjustment, unlike $n = 1$ phasing to be discussed in the next section, is very limited to either even or odd parities between adjacent rows.

3.2. Phasing dependence and robust RMP-driven ELM-crash-control

One of the important goals in RMP physics is not only to achieve the ELM suppression, but also to secure a reliable path to it. Since an optimal phasing was reported to be quite critical in suppressing ELMs using $n = 2$ RMP in DIII-D [29],
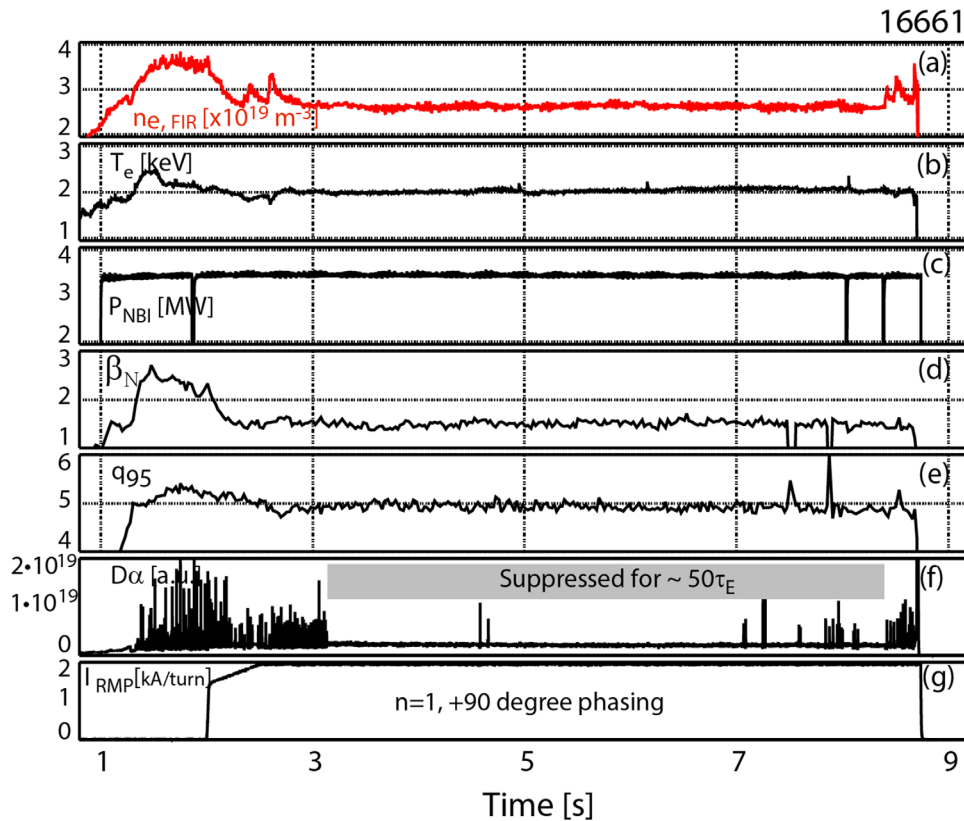
Figure 4. RMP-driven ELM-crash suppression with an optimal *X*-point for divertor heat flux study. Shown are the time traces of (a) density, (b) core electron temperature, (c) NBI power, (d) normalized β, (e) safety factor, q_{95}, (f) D_α signal at divertor, and (g) RMP coil current per turn.
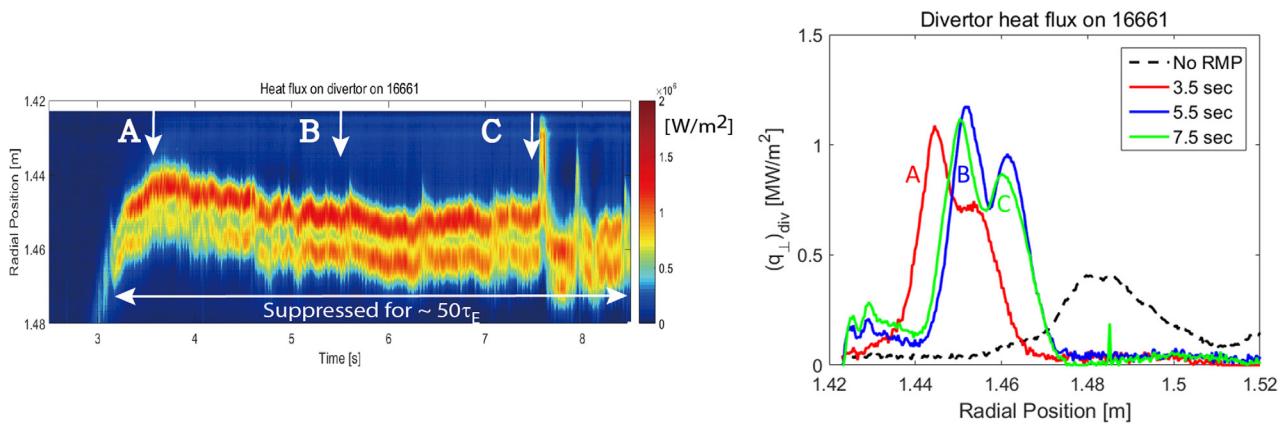

Figure 5. Divertor heat flux during ELM-crash-suppression. (Left) Shown is the time evolution of the divertor heat flux measured during the $n = 1$ RMP-driven ELM-crash-suppression (with peaks mostly below 1.2 MW m^{-2}). (Right) Shown are the radial profiles of divertor heat flux at the denoted times of 3.5, 5.5 and 7.5 s on 16661 respectively, in comparison with other discharge with no RMP (dashed).

the $n = 1$ phasing dependence in KSTAR has been systematically investigated.

Although the $n = 1$, $+90°$ phasing is known to be quite effective in KSTAR, that may not warrant it would be the most optimal for various plasma conditions (e.g. q_{95} or edge collisionalities (ν^*) etc). Thus, assuming that resonant components in an optimal RMP phasing should be configured (i) maximally at the edge to control ELMs [$\sum_{edge}(\delta B)$] but (ii) minimally in the core to avoid mode-locking [$\sum_{core}(\delta B)$], a systematic map of the ratio of these two quantities [$\sum_{edge}(\delta B)/\sum_{core}(\delta B)$] has

been established in vacuum and ideal plasma response modelling, using IPEC [26], as summarized in the polor plots of (I_{MID}, ϕ) in figure 6. With top/bottom rows fixed at 5 kA/turn (effective; 10 kA), the phasing (ϕ) between rows is shown counterclockwise, while the radius (I_{MID}) of the circle represents the current amplitude at the middle row. According to the vacuum and ideal plasma response calculations, depending on the phasing, there are three distinctive bands (locking(brown), non-resonant(green) and suppression(blue)). To validate whether a proper level of RMP currents for ELM suppression and mode-locking would exist at a specific phasing, one
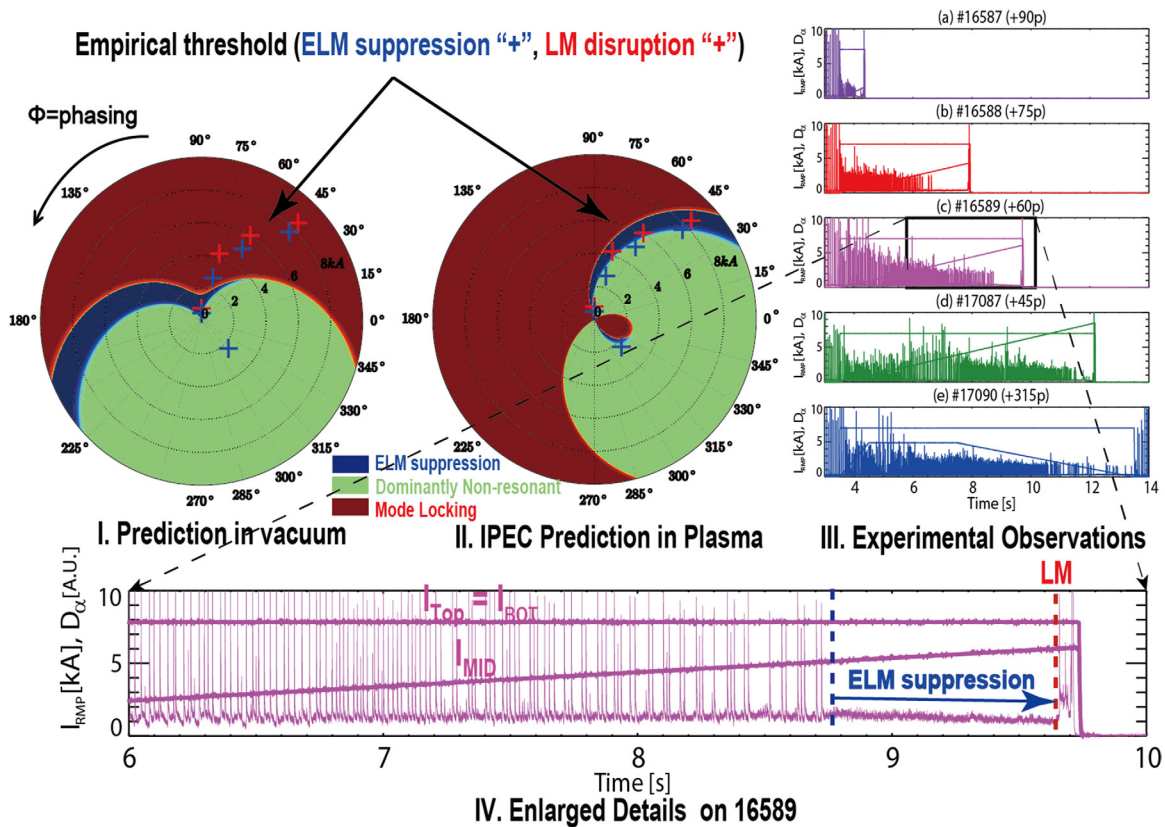
Figure 6. Polar plots (I_{MID}, ϕ) for phasing dependence of $n = 1$, RMPs in KSTAR in vacuum (I) and plasma (II) respectively, along with the time-evolutions of RMP coil currents and D_α (III and IV). With top/bottom rows fixed at 10 kA (5 kA/turn, effective), the phasing (phase difference between rows) is marked in polar angle (ϕ), while the radius (I_{MID}) represents the mid-plane RMP current. The blue band indicates the predicted the ELM suppression windows in I and II. In III and IV, shown are the shot traces with each of the fixed phasing, demonstrating the existence of ELM suppression threshold ('+' in blue) and locked mode disruptions ('+' in red), whose experimental points are individually denoted in I and II. While higher RMP currents lead to mode locking, clear phasing-dependent ELM suppression window has been identified. It is to be noted that vacuum calculation prediction in I was grossly misleading, while the IPEC prediction in II was quite consistent with the experimental observations.

of the well diagnosed discharges, similar to the discharge in figure 2, was referenced. That is, the ELM suppression is predicted in the window defined by $\sum_{edge}(\delta B) > [\sum_{edge}(\delta B)]_{Ref}$, while keeping $\sum_{core}(\delta B) < [\sum_{core}(\delta B)]_{Ref}$, as the I_{MID} varies. Then, a set of experiments was conducted to test this newly predicted ELM suppression window (in blue on I and II in figure 6), by varying I_{MID} in each of the fixed phasings at (a) 90 (b) 75 (c) 60 (d) 45 and (e) 315 (°). The experiments indeed demonstrated the existence of the ELM suppression windows in the predicted range of currents at all the tested phasings, as summarized in the middle figure of figure 6 with the experimental results on ELM suppression and locked mode disruption. The agreement shown here with ideal 3D response is quite remarkable, given the narrowness of the windows in such a large coil configuration.

Interestingly, it is to be noted that a non-conventional phasing (e.g. 315° in figure 6(e)), which we rarely pay attention to, tends to follow the modeling prediction, as well. To access the ELM suppression window without mode-locking, the RMP current has been arranged to be reduced from high currents, rather than increased from low currents (compared to other phasings). Without having an ideal plasma response prediction, it was very unlikely that we would have attempted

the dominantly non-resonant phasing (equivalent to $-45°$ phasing), which would be almost orthogonal to a typical phasing (i.e. near $+90°$ phasing). Surely, this new modelling capability is expected to help us chart a new route even to a seemingly unlikely phasing, including other unexplored 3D configurations. Meanwhile, the vacuum superposition method critically failed in the prediction, as shown in the left figure of figure 6. The importance of plasma response on the RMP ELM control has been recently highlighted in the DIII-D [29], but this investigation consolidates their findings with the greatly improved isolation of plasma response using 3 rows of coils. The details will be reported elsewhere [30].

3.3. Non-axisymmetric field dependence of power threshold for L–H transition

Since the introduction of non-axisymmetric field (δB) for RMP-driven ELM control affects the power thresholds (P_{th}), a very systematic study was conducted in DIII-D, showing that unless the RMP strength gets high, there would be minimal impact on P_{th} for L–H transition [31]. Ever since, many other devices reported a similar trend of P_{th}, which appears insensitive in low δB, but linearly increasing in high δB. However,
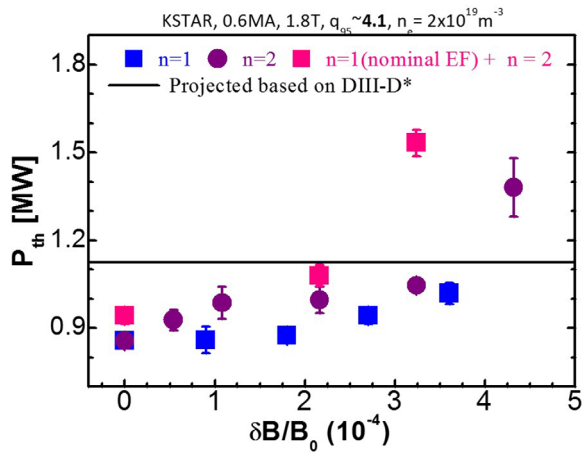
Figure 7. Power thresholds (P_{th}) dependence on non-axisymmetric fields. Shown are the dependences of $n = 1$ (blue square), $n = 2$ (purple circle), and $n = 2$ on top of a fixed $n = 1$ field (magenta square) respectively. Note that the error bars are quite small in a majority of the discharges, except for a few cases. *Projected with reference to DIII-D data [31] using an empirical scaling law [33].

considering that KSTAR has a much lower level of $n = 1$ intrinsic EF than other tokamaks, any accumulative effects of 'uncorrected' multiple low-n intrinsic EFs are expected to be also minimal in KSTAR. Figure 7 shows the measurement results based on three sets of non-axisymmetric fields. As a result, the $n = 1$ δB shows a very weak linear dependence at low δB, while showing a slightly stronger linear dependence at high δB. However, the $n = 2$ δB shows a strongly linear dependence even at low δB, an insensitivity at the intermediate δB, but a strongly linear dependence at high δB. To address any merit of low non-axisymmetric field in KSTAR, we added an $n = 1$ field that would be equivalent to a typical $n = 1$ intrinsic EF in conventional devices (e.g. nominal $n = 1$ $\delta B/B_0 \sim 2.7 \times 10^{-4}$ at edge, where pedestal top could be formed) on top of $n = 2$ field scan. It turns out that such a mixed δB (magenta square) leads to much higher P_{th}, once $n = 2$ gets higher than $\delta B/B_0 \sim 2.2 \times 10^{-4}$, resulting in $P_{th} \sim$ 1.5 MW. This suggests that due to multiple 'uncorrected' EFs in tokamaks, the power threshold P_{th} would get much higher than what a single non-axisymmetric field could dictate.

As a note, the previous study in DIII-D reported $P_{th} \sim$ 1.6 MW ($n_e = 0.29 \times 10^{20}$ m^{-3}, $B_T = 1.7$ T, $S = 56$ m^2) [31], while its standard $n = 1$ EF correction was applied without $n = 3$ RMP [32]. However, it is ~19% higher than the estimation using Martin's scaling law $P_{th, Martin} = c\, n_{e20}^{0.72}\, B_T^{0.80}\, S^{0.941}$, where $c = 0.049$ [33] ($P_{th, Martin} = 1.35$ MW). Here, S refers to the surface area of plasma boundary. Meanwhile, the power threshold without RMP in KSTAR was $P_{th} = 0.86$ MW ($n_e = 0.2 \times 10^{20}$ m^{-3}, $B_T = 1.8$ T, $S = 49$ m^2), which is ~9% lower than the estimation of 0.95 MW. Since all the three plasma parameters (n_e, B_T, S) in two devices vary somewhat, it may not be straightforward to make a direct comparison between DIII-D and KSTAR experimental results. Thus, assuming the DIII-D experimental result is the reference that has a higher coefficient than that of Martin's scaling law ($c' = (1.6$ MW/1.35 MW$)c$), the KSTAR experimental conditions can be projected to 1.13 MW, as drawn in horizontal line in figure 7. It is to be noted that the

multi-device empirical scaling [33] has no δB dependence and that KSTAR has approximately 24% lower P_{th} than the projection that is based on a similar discharge in DIII-D. Overall, this suggests that the merit of low intrinsic EFs on P_{th} might have been inadvertently overlooked in previous studies. Specifically, owing to the presence of multiple 'uncorrected' intrinsic EFs, it is possible that the experimental results on P_{th} dependence might not have been sufficiently resolved in the existing devices. Therefore, the lower P_{th} in KSTAR could be attributable to low level of intrinsic non-axisymmetry, which is likely due to not only low $n = 1$ δB, but also possibly other low $n > 1$ δB harmonics that have not been measured yet. At the same time, one needs to be reminded that the non-axisymmetric field influence alone cannot explain the large scatters shown in the worldwide database used in the establishment of Martin scaling [33], which requires separate extensive studies in multiple devices.

4. Intentionally misaligned RMP impacts on divertor heat flux footprints

To support the ITER RMP study, both $n = 1$ and $n = 2$ RMP configurations have been extensively tested in KSTAR with two approaches; (1) switching low-n RMPs during ELM-suppressed stage, and (2) intentionally misaligned RMP configurations. Primarily, both of these approaches have been proposed to address whether localized divertor heat flux loads could be effectively redistributed by RMPs in ITER. Unfortunately, the approach (1) was operationally limited due to an axisymmetric control need to switch the safety factor q_{95} between $n = 1$ ($q_{95} = 5$) and $n = 2$ ($q_{95} = 3.9$), aside from the difficulty of getting $n = 2$ RMP-driven ELM-crash-suppression. But, the approach (2) has been greatly substantiated, measuring the divertor heat flux striation patterns in strongly ELM-mitigated phases during static and rotating misaligned RMP configurations.

4.1. ELM-mitigation with intentionally misaligned RMP configurations

Figure 8 shows the time evolution of various plasma parameters on discharge (16822) with intentionally misaligned RMP configurations, while figure 9 shows the details of RMP amplitude, phase and phasing in the relevant RMP configurations. Considering that full ELM-crash-suppression was achieved at $n = 1$, $+90°$ phasing (compatible with the divertor-camera view, as shown in figures 4 and 5), the misalignment has been imposed on top and bottom rows with respect to mid-row by 5° increment and decrement respectively, as defined at the bottom of figure 9. Specifically, the phasing between top and mid rows increases every 2 s, while the counterpart between mid and bottom rows decreases at the same time. Thus, with the phase of mid-row fixed at 0 (°), the toroidal phases of top and bottom rows are configured at (ϕ_{Top}, ϕ_{Bot}) = ($-95, +85$), ($-100, +80$), ($-105, +75$) and ($-110, +70$) (°) successively, rather than at a fixed (ϕ_{Top}, ϕ_{Bot}) = ($-90, +90$) (°). (Since the phasing is defined as the phase difference between upper and lower rows, the $n = 1$, $+90$ phasing corresponds to the toroidal phases of ($\phi_{Top}, \phi_{Mid}, \phi_{Bot}$) = ($-90, 0, +90$) (°) in
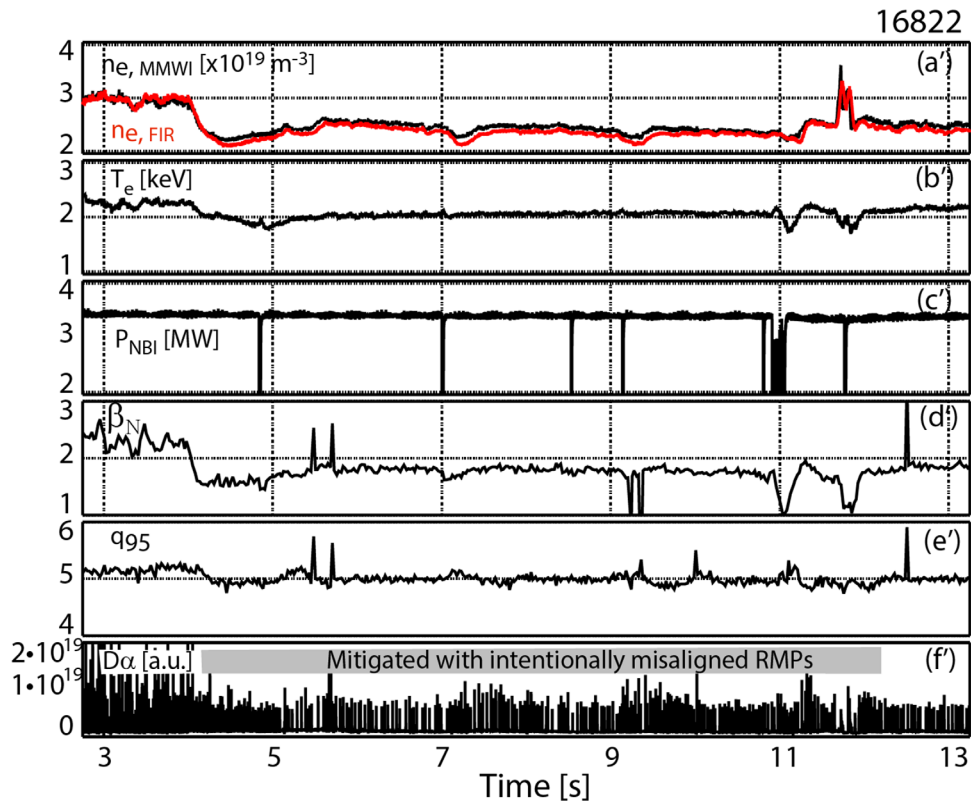
Figure 8. ELM-crash-mitigation with intentionally misaligned RMP configuration. Shown are the time traces of (a′) density, (b′) core electron temperature, (c′) NBI power, (d′) normalized β, (e′) safety factor, q_{95}, and (f′) D_α (lowest-energy spectral line of deuterium Balmer series) signal at divertor.

standard configuration in KSTAR, for example.) Also, at a given misaligned phasing, both static and rotating RMPs have been configured to be sustained for 1 s respectively. The main purpose of a rotating RMP is to diagnose the toroidally asymmetric divertor heat flux footprints that cannot be accessed by the toroidally fixed divertor camera with static RMP.

4.2. Divertor heat flux footprints

Figure 10 shows the time evolution of divertor heat flux footprints and divertor D_α signal, along with the profiles at a few timeslices of interest respectively. Despite no full suppression of ELMs, the striation patterns of ELM mitigation appear quite similar to those of ELM suppression, except the peak of non-axisymmetric lobe. Specifically, in comparison with figure 5 that has full ELM-crash-suppression, the axisymmetric peaks during ELM-crash-mitigation remain at a similar level of below ~1.2 MW m^{-2}, though the non-axisymmetric peak has been reduced by almost a half (down to ~0.5 MW m^{-2}) in figure 10. When comparing various divertor heat flux profiles in static misaligned RMP configurations (right figure of figure 10), it is not difficult to conclude that the divertor heat flux peaks and widths get lower and broadened respectively, as the degree of misalignment (i.e. dephasing) increases.

4.3. Comparison of static and rotating RMP configurations

Since such static RMP results cannot capture any toroidally asymmetric heat flux footprints properly, a toroidal average
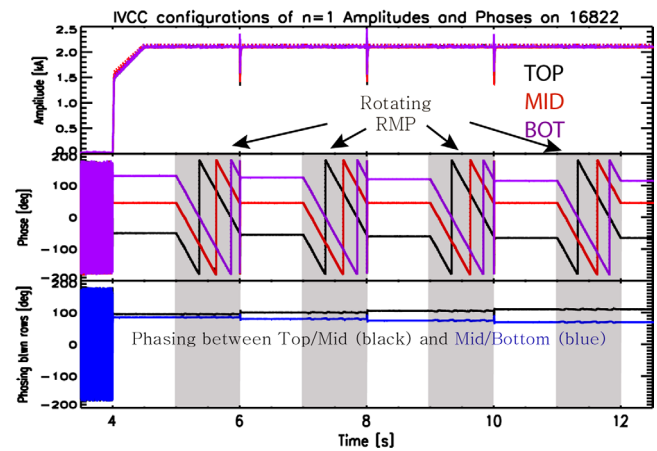

Figure 9. Schematic of the intentionally misaligned RMP configuration for ITER. From the top are the time traces of RMP current amplitude per turn, toroidal phase, and absolute phasing between rows. Four types of misaligned RMP configurations are applied to be either static or rigidly rotating (shaded).

of rotating RMP would be of great help to confirm the validity of the static RMP results. In fact, the left figure of figure 11 shows such toroidally-averaged divertor heat flux at each rotating misaligned RMP configuration. As expected, the toroidal average removes the non-axisymmetric lobes but the toroidally averaged axisymmetric lobe appears less peaked with broader width, corroborating the static RMP analysis results shown in figure 10. Meanwhile, it is much more important to compare the normalized shapes of divertor heat fluxes at various RMP configurations, when the RMP
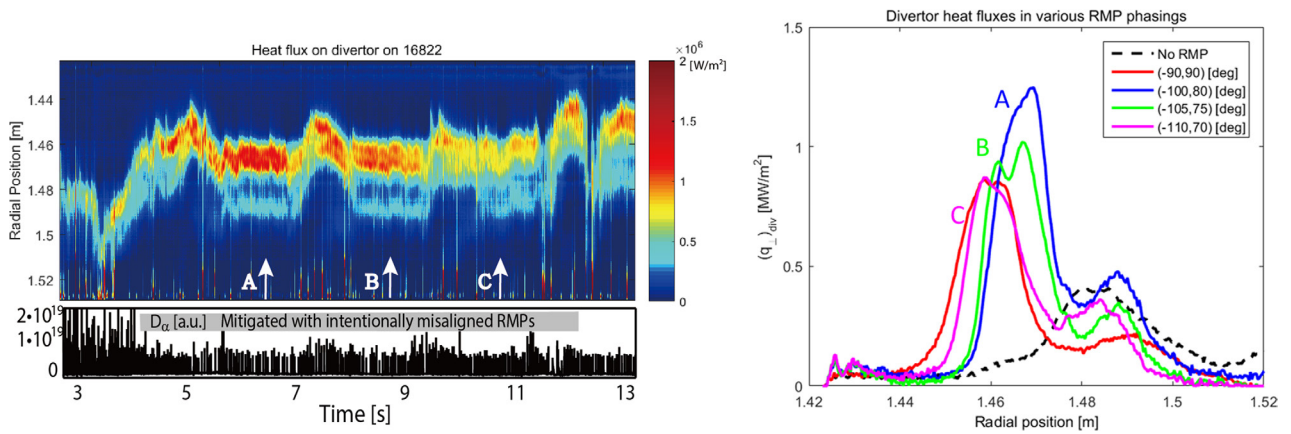
Figure 10. Divertor heat flux during ELM-crash-mitigation in four types of misaligned RMP configurations. On the left are the time evolutions of the measured divertor heat flux with 4 types of RMP configurations (either static or rotating), along with divertor D_α signal. On the right are the divertor heat flux profiles during static RMP-driven ELM-crash-mitigation at each time slice denoted by A, B, and C with arrows, in which (ϕ_{Top}, ϕ_{Bot}) refers to the phases of top and bottom row.
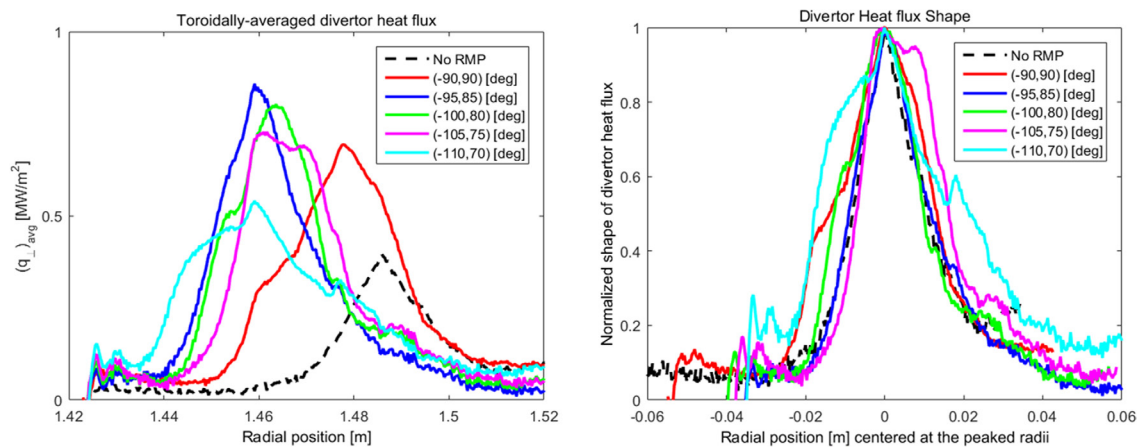

Figure 11. Toroidally-averaged divertor heat fluxes and their shapes in misaligned rotating RMP configurations. On the left are the profiles of toroidally-averaged divertor heat flux in each misaligned rotating RMP configuration, in comparison with no RMP (black) and a typical rotating RMP with $n = 1$, $+90°$ phasing (red). On the right are the corresponding normalized shapes of divertor heat flux at each configuration. Here, (ϕ_{Top}, ϕ_{Bot}) refers to the phases of top and bottom row, while fixing ϕ_{Mid} at 0 (°).

applicability to ITER and future devices is concerned. For that reason, the right figure of figure 11 confirms the effectiveness of the intentionally misaligned RMP configurations, where the increase of misalignment leads to a broadened heat flux shape. Technically, the misaligned RMP configurations can be easily realized to reduce the localized heat flux loading without resorting to any special hardware other than independent phase control capability at each row (which is already planned to be equipped in ITER). Once such a favourable outcome is consistently reproduced even during RMP-driven ELM-crash-suppression, various concerns related to time-varying RMP application would be significantly alleviated in ITER and future reactors.

Nevertheless, we are aware that the RMP alone might not be sufficient to reduce the axisymmetric peak divertor heat flux, but that other means, such as detached plasmas, should be vigorously explored, as well. To be fair, multiple non-axisymmetric lobes induced by higher non-axisymmetric harmonics would be also of help to redistribute the divertor heat flux in a wider area, while the RMP application needs to avoid mode-locking at the plasma core.

5. Discussion

When intrinsic non-axisymmetric fields are essentially none or little, the uncertainties of non-axisymmetric field physics research can be also minimized. In that view, KSTAR, which has an order of magnitude lower level of intrinsic non-axisymmetric fields than other tokamaks, is ideally positioned to unambiguously address the relevant 3D physics. The first demonstration of $n = 1$ RMP-driven, ELM-suppression in KSTAR [27], which many existing devices cannot still access, was quite intriguing but may be now easily understood as one of the meritorious benefits of low intrinsic non-axisymmetry. Specifically, in KSTAR, the applied $n = 1$ RMP can be increased large enough to suppress ELMs without invoking kink-dominant mode-locking that otherwise might have plagued the plasmas, as seen in many other devices [10]. In fact, a recent success of $n = 1$ RMP-driven ELM suppression in EAST [34], whose intrinsic $n = 1$ EF is also in the order of $\delta B/B_0 \sim 10^{-5}$ [35], supports such a leading hypothesis made in KSTAR. Also, the recent sustainment of ELM-suppression with a fully rotating $n = 1$ RMP in KSTAR might not have

been possible, if the intrinsic $n = 1$ EF level had not been in a negligible level [19].

Thus, it is quite reasonable to assume that RMP-driven ELM suppression would require maximal δB at edge (to drive stochastic fields) but minimal δB in core (to avoid mode-locking). Using such a rather simple guideline, an ideal plasma response modeling helped us to theoretically map out both ELM suppression and mode-locking conditions in advance, which turned out to be in excellent agreement with the experimental outcome [30]. Overall, the IPEC calculations proved to be quite effective in predicting a global eigenmode structure with respect to ideal plasma response, which could not be so sensitive to the details of edge equilibrium profiles. Thus, this suggests that we need to investigate global plasma response and influences in RMP ELM physics in high priority, as well as to look into edge profile variations.

Meanwhile, there are several points about RMP-driven ELM control physics we may need to address. First, the shape dependence of R_x (equivalent to δ_l) needs to be further examined. Unlike strong R_x dependence, no Z_x dependence has been noticed in the experiments. Considering that both elongation and triangularity are quite critical to determine peeling-ballooning stability boundaries (e.g. [36]), such contrasting dependence of R_x and Z_x needs to be clarified.

Second, there seem to be multiple optimal windows of R_x dependence, whose sensitivities vary significantly. Specifically, while the 'performance-oriented' configuration (e.g. 15433) was accompanied by $\Delta R_x = \pm 0.02$ m ($\Delta \delta_l = \pm 0.04$), $\Delta q_{95} = \pm 0.25$, the 'divertor-camera constrained' configuration (e.g. 16661) was substantially (more than a factor of 2) limited by $\Delta R_x = \pm 0.01$ m ($\Delta \delta_l = \pm 0.02$), $\Delta q_{95} = \pm 0.05$. This suggests that historically narrow q_{95} dependence might also accompany additional window, whose constraints can be more relaxed, subject to the choice of key shape parameter (e.g. R_x).

Third, the effectiveness of intentionally misaligned RMP configuration needs to be examined until it becomes ineffective. In comparison with an optimal phasing (i.e. $n = 1$, $+90°$ phasing), each misaligned RMP configuration is expected to lead to a weaker plasma response, eventually incapable of affecting the ELMs at the extreme phasing. Also, since plasma response is expected to be stronger in ELM-suppression rather than in ELM-mitigation, an effective range of misalignment in ELM suppression may appear different from what has been found in ELM mitigation. In particular, since such ITER-like 3-row variations cannot be accommodated in other major tokamaks, the additional experiments in KSTAR are deemed essential to clarify any benefits of misalignment for ITER.

Although the details have not been presented here, we have confirmed a clear β-dependence of optimal RMP strength for ELM suppression, requiring a reduced δB in high-β plasma [19]. Specifically, in high-β plasmas with 3 neutral beam injectors (NBI) at $\beta_N \sim 2$, the optimal level of RMP currents was found to be ~20% lower than in intermediate-β plasmas with 2 NBIs at $\beta_N \sim 1.6$ [19]. Such β-dependence can be also interpreted in terms of ν^* dependence, in that a low ν^* in high-β plasma requires a reduced RMP strength [19]. Such β and ν^*

dependence proved to be quite critical to design various high performance discharges, whose evolution and sustainment are greatly subject to various plasma responses against controlled non-axisymmetric fields. For example, it is not uncommon in KSTAR to use both resonant and non-resonant magnetic perturbations to adjust the L–H transition timing, as well as to control plasma rotation.

6. Summary

The uncertainties of non-axisymmetric field physics are expected to be better resolved, when the intrinsic components do not compete with controlled counterparts. Such an ideal environment for non-axisymmetric field study has been recognized in KSTAR ($\delta B/B_0 \sim 10^{-5}$), which has an order of magnitude lower intrinsic EF than conventional devices ($\delta B/B_0 \sim 10^{-4}$). A systematic study shows that the $n = 1$ intrinsic non-axisymmetric field in KSTAR remains as low as $\delta B/B_0 \sim 4 \times 10^{-5}$ even at high-β plasmas ($\beta_N \sim 2$), which corresponds to approximately 20% below the targeted ITER tolerance level. Among various controlled non-axisymmetric field (δB) studies, the KSTAR has made outstanding progress on RMP physics and P_{th} study. Specifically, as for the RMP-driven ELM control, robust $n = 1$ RMP ELM-crash-suppression has been not only sustained for more than ~90 τ_E, but also confirmed to be compatible with rotating RMP. Throughout this study, we have found the optimal window of radial position of lower X-point, whose role has been found to be as pivotal as that of q_{95}. At the same time, there is an evidence that there could be multiple windows that could be not accessible directly from one set of plasma parameters, but approachable from the other neighboring set of conditions. Also, we have addressed the importance of optimal phasing for $n = 1$ RMP-driven ELM control, consistent with ideal plasma response modeling which could predict both ELM suppression and locking thresholds. On the other hand, in ITER-like 3-row RMP configurations, intentionally misaligned RMPs have been found to be effective in mitigating ELMs, in which divertor heat flux peak patterns (up to ~1.2 MW m^{-2} in axisymmetric lobe, ~0.5 MW m^{-2} in $n = 1$ lobe) were measured similarly to what ELM-crash-suppression has accompanied (up to ~1.2 MW m^{-2} in both lobes). Further study may need to combine RMP with other means, such as detached plasmas, so that even the axisymmetric peaks can be lowered. Besides, a systematic survey of P_{th} dependence on non-axisymmetric field has revealed that the KSTAR has lower P_{th} than projected by a multi-device empirical scaling, attributable to a low level of intrinsic non-axisymmetry. A weak but solidly linear trend of δB even at low δB in KSTAR should be explored further to understand the long-standing mystery of L–H transition physics. Since the planned ITER RMP coils are composed of 3-rows, just like in KSTAR, further controlled non-axisymmetric field physics study in KSTAR is expected to help us resolve the uncertainties of the ITER RMP coils (in particular, related to in-vessel mid-plane coils), as well as establish the optimal 3D configuration for ITER and future reactors.

Acknowledgments

ITER disclaimer

The views and opinions expressed herein do not necessarily reflect those of the ITER Organization

References

[1] Boozer A.H. 2001 *Phys. Rev. Lett.* **86** 5059
[2] Garofalo A.M. *et al* 2007 *Nucl. Fusion* **47** 1121
[3] Evans T.E. *et al* 2004 *Phys. Rev. Lett.* **92** 235003
[4] Hender T.C. *et al* 2007 *Nucl. Fusion* **47** S128
[5] Doyle E.J. *et al* 2007 *Nucl. Fusion* **47** S18
[6] Boozer A.H. 2011 *Fusion Sci. Technol.* **59** 561
[7] Buttery R.J. *et al* 2012 *Phys. Plasmas* **19** 056111
[8] Loarte A. *et al* 2014 *Nucl. Fusion* **54** 033007
[9] Park J.K. *et al* 2007 *Phys. Rev. Lett.* **99** 195003
[10] In Y. *et al* 2015 *Nucl. Fusion* **55** 043004
[11] Yoon S.W. *et al* 2014 Overview of KSTAR results in 2013 campaign paper presented at *25th IAEA Int. Conf. on Fusion Energy, (St Petersburg, Russia 2014)* [OV/3-4]
[12] In Y. *et al* 2017 to be published
[13] Piovesan P. *et al* 2014 *Phys. Rev. Lett.* **113** 04500
[14] Kim J. *et al* 2015 Exploration of low q_{edge}/q_{95} regime in KSTAR *25th ITPA Topical Group Meeting on MHD and Disruption (Cadarashe, France)*
[15] Lee S.G. *et al* 2017 submitted
[16] Lee H.H. *et al* 2016 *Phys. Plasmas* **23** 082510
[17] Yun G.S. *et al* 2012 *Phys. Plasmas* **19** 056114
[18] Lee J. *et al* 2016 *Phys. Rev. Lett.* **117** 075001
[19] Jeon Y.M. *et al* 2016 Robust RMP-ELM control with distinctive optimization of plasma shape in KSTAR *Preprint: 2016 IAEA Fusion Energy Conf. (Kyoto, Japan)* [PDP-1]
[20] Ko W.H. *et al* 2016 Influences of non-axisymmetric field on H-mode power threshold and pedestal rotation in KSTAR *Preprint: 2016 IAEA Fusion Energy Conf. (Kyoto, Japan)* [EX/P4-4]
[21] Kim H.K. *et al* 2009 *Fusion Eng. Des.* **84** 1029
[22] Han H.S. *et al* 2016 *Fusion Eng. Des.* **108** 66
[23] Lee W.C. *et al* 2014 *Nucl. Fusion* **54** 023012
[24] Reimerdes H. *et al* 2012 Rotation braking and error field correction of the test blanket module induced magnetic field error in ITER *Proc. 24th Int. Conf. on Fusion Energy (San Diego, 2012)* [EX/P4–09] (www-naweb.iaea.org/napc/physics/FEC/FEC2012/index.htm)
[25] Wang Z.R. *et al* 2015 *Phys. Rev. Lett.* **114** 145005
[26] Park J.K., Boozer A.H. and Glasser A.H. 2007 *Phys. Plasmas* **14** 052110
[27] Jeon Y.M. *et al* 2012 *Phys. Rev. Lett.* **109** 035004
[28] Lee H.H. *et al* H-mode divertor target heat load measurements on KSTAR *Preprint: 2016 IAEA Fusion Energy Conference (Kyoto, Japan)* [EX/P4-24]
[29] Paz-Soldan C. *et al* 2015 *Phys. Rev. Lett.* **114** 105001
[30] Park J.K. *et al* 2017 submitted
[31] Gohil P. *et al* 2011 *Nucl. Fusion* **51** 103020
[32] Gohil P. 2016 private communication
[33] Martin Y. *et al* 2008 *J. Phys.: Conf. Ser.* **123** 012033
[34] Sun Y. *et al* 2016 *Phys. Rev. Lett.* **117** 115001
[35] Wang H. *et al* 2016 *Nucl. Fusion* **56** 066011
[36] Snyder P.B. *et al* 2004 *Nucl. Fusion* **44** 320